View metadata, citation and similar papers at core.ac.uk
brought to you by CORE
provided by Elsevier - Publisher Connector

Available online at www.sciencedirect.com

ScienceDirect

Procedia Structural Integrity 2 (2016) 1015–1022

Structural Integrity Procedia

www.elsevier.com/locate/procedia

21st European Conference on Fracture, ECF21, 20-24 June 2016, Catania, Italy

# Modelling of Phased Array Ultrasonic Inspection of a Steam Generator Dissimilar Metal Weld

Szabolcs Szávai[a,*], Zoltán Bézi[b], Judit Dudra[c], István Méhész[d]

[a]*Head of Department, Iglói street 2., Miskolc 3519, Hungary**
[b, c]*Research Fellow, Iglói street 2., Miskolc 3519, Hungary**
[d]*Head of Laboratory, Iglói street 2., Miskolc 3519, Hungary**
**Bay Zoltán Nonprofit Ltd. for Applied Research, Engineering Division (BAY-ENG)*

**Abstract**

Phased array ultrasonic techniques (PAUT) are more and more used for inspection of the primary circuit of nuclear power plants in order to detect defects such as stress corrosion cracking (SCC) at the dissimilar metal welds (DMWs) between the main pipe lines and large components such as the pressure vessel, steam generators and pressurizers. Nevertheless, disturbances such as beam splitting and skewing may occur due to the anisotropic and inhomogeneous properties of the welding material. These disturbances affect the detection, localization and sizing of possible weld discontinuities. Simulation tools can help to understand these physical phenomena, optimize ultrasonic testing. Since strict safety requirements are leading to increased demands for the inspection of such components, a research task called MAPAID has been dedicated under the umbrella of "NUGENIA+" FP7 project to model and validate PAUT techniques for inspection of DMWs of nuclear power plants. As a part of the task, this study presents the phased array ultrasonic inspections and ultrasonic simulations of steam generator DMW. The testing has been recently developed in the CIVA in order to determine the index distances regarding the given orientation artificial defect analysis and the incident angles for longitudinal and transversal tests. By comparing the experimental and simulation tests results, conclusions can be drawn to quantitatively assess the contribution of phased array techniques to improved NDE performances of such parts, as well as the ability of simulation to help for design, optimization and interpretation of such inspections.

Copyright © 2016 The Authors. Published by Elsevier B.V. This is an open access article under the CC BY-NC-ND license (http://creativecommons.org/licenses/by-nc-nd/4.0/).
Peer-review under responsibility of the Scientific Committee of ECF21.

*Keywords:* Steem generator, dissimilar metal weld, DMW, phased array ultrasonic inspection, PAUT;

* Szabolcs Szávai. Tel.: +36-70-205-6455; fax: +36-46-422-786.
*E-mail address:* szabolcs.szavai@bayzoltan.hu

Copyright © 2016 The Authors. Published by Elsevier B.V. This is an open access article under the CC BY-NC-ND license (http://creativecommons.org/licenses/by-nc-nd/4.0/).
Peer review under responsibility of the Scientific Committee of ECF21.
10.1016/j.prostr.2016.06.130

## 1. Introduction

In a nuclear power plant, a single metallic component may be fabricated from different materials. For example, the steam generators of nuclear power plants are made of ferritic steel, whereas some of the connecting pipelines are fabricated from austenitic stainless steel. As a consequence different components often need to be connected by so-called dissimilar metal welds (DMW). DMWs are used because of their high fracture toughness, resistance to corrosion and creep at elevated temperatures, but their structural stability is strongly affected by welding conditions and post weld heat treatment. DMWs on the lower part of the steam generator collectors of nuclear power plants have shown a significant damage in several nuclear power plants in the last third of their design life (Fig. 1.). The damage phenomenon is intergranular corrosion attack starting from the internal surface which leads to loss of cohesion of grain boundaries between ferritic collector material and the first layer of the buttering, and then to a large discontinuity. The damage may occur along the whole circumference, its depth can vary. Thus, it is very important to evaluate the structural integrity of these materials using highly reliable non-destructive testing (NDT) methods.

Ultrasonic techniques are extensively used during in-service inspections of components of nuclear power plants, because of their capabilities to detect and size potential in-depth flaws. Phased array ultrasonic techniques (PAUT) offer significant technical advantages for weld inspections over conventional ultrasonic. The phased array beams can be steered, scanned, swept and focused electronically. Beam steering permits the selected beam angles to be optimized ultrasonically by orienting them perpendicular to the predicted defects. The inspection of dissimilar weld components is complicated because of anisotropic and inhomogeneous properties of the welding materials leading to beam splitting and skewing. These disturbances affect the detection, localization and sizing of possible weld discontinuities. Simulation tools are able to help to optimize ultrasonic NDT and play an important role in developing advanced reliable ultrasonic testing (UT) techniques and optimizing experimental parameters for inspection of dissimilar weld components.

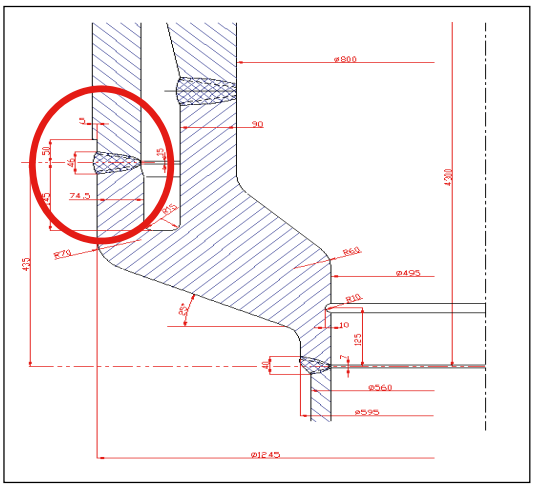


Fig. 1. Dissimilar metal weld of the steam generator collector.

In this paper, the phased array ultrasonic testing of DMWs is investigated by experimental and computer simulation. The DMW specimen will first be examined for their weld structure including degree of anisotropy and grain orientation distribution. The flawed welded specimen is prepared by SAW and GTAW welding processes. The base and weld materials, geometry of the bevel, and implanted artificial defects are identical. A two-dimensional axisymmetric thermal-mechanical finite element (FE) model has been developed to investigate the local grain direction of the weld material and they coupled the results of the FE model with commercial ultrasonic modeling software tool (CIVA) to predict the ultrasound propagation in the DMW of the steam generator collector. This CIVA model has been applied on a weld described as a set of several homogeneous domains with a constant

crystallographic orientation. The results of UT analyses and the detection of flaws located in the weld and the buttering were compared directly to experimental results for different testing configurations on the specimen with phased-array probes.

## 2. Characterization of DMWs

DMW specimen comes from decommissioned non-operated VVER 440 reactor. DMW is used to join low alloy carbon steel nozzle and stainless steel collector. Originally, steel 22K was the manufacture material for the nozzle of steam generator. The safe-ends of nozzles were manufactured from austenitic steel 08H18N10T. The base materials are widely different so in order to perform the welding a transient buttering or cushion has to be implemented. Two high alloyed buttering layers EA-395/9, Sv-04CH19N11M3 and filler metal EA-400/10T were used (Fig. 2.).

In welding, as the heat source interacts with the material, resulting in three distinct regions in the weldment. These are the fusion zone, also known as the weld metal, the heat affected zone, and the unaffected base metal. The fusion zone is created by heating above the melting point during welding process. The weld microstructure development in the fusion zone is more complicated because of physical processes that occur due to the interaction of the heat source with the metal during welding, including re-melting, heat and fluid flow, vaporization, dissolution of gasses, solidification, subsequent solid-state transformation, stresses, and distortion. These processes and their interactions profoundly affect weld pool solidification and microstructure. During the solidification process, the austenitic phase forms long columnar grains which grow along the directions of maximum heat loss during cooling. The extensive columnar grain structure in some austenitic welds differs greatly from that in ferritic welds. Generally, during the process of welding, beads are produced, in which grains grow along the maximum thermal gradient when cooling. In an austenitic weld, the deposition of succeeding weld beads does not destroy the grain structures in the previous beads, the columnar grains then grow through the boundaries of the beads. Consequently, grains of substantial length are produced by Kolkoori (2014) and Moysan et al. (2003). A macrograph of a typical DMW is shown in Fig. 2.b.

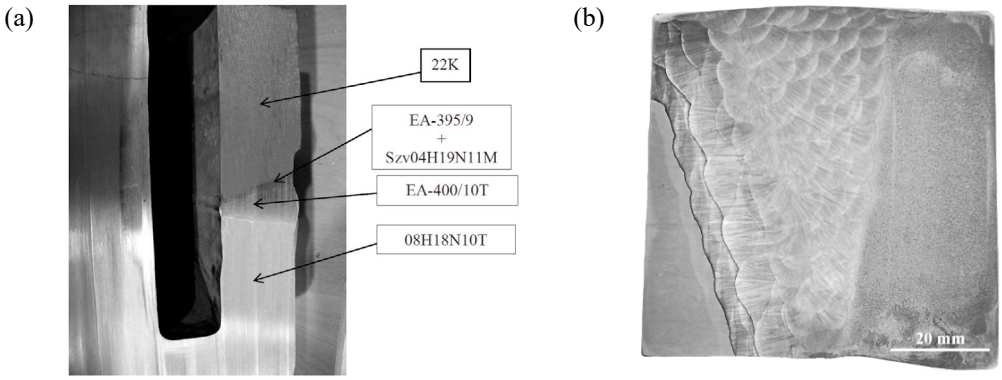


Fig. 2. (a) Materials of DMW specimen; (b) Typical macrograph by Skoumalová (2014) et al .

In order to analyze the effect of welding process on the microstructure of the girth welds numerical models must be used. The microstructure of the welded joint depends heavily on the base metal structure. So it is important to know the welding method and the effects of the different regions on the resulting microstructure. The DMW specimen under investigation (Fig. 1-3.) has a V-shaped chamfer filled with 49 weld passes. The girth welded specimens were prepared by SMAW and GTAW welding processes. The thickness of base material, root gap and bevel angels were 70, 5mm, 10° and 15°, respectively. The root pass was done by GTAW, and the remaining passes by SMAW process. The diameters of the electrodes were 1.6mm in the first layer and 2mm in other layers.

The parameters directly used in the modelling will be the number and the order of passes and the diameter of the electrodes. In present numerical simulation only the girth welding process has been modeled to investigate their local grain structure.

Numerical calculations were performed with commercial finite element (FE) software package MSC. Marc. The problem was solved numerically in a cylindrical coordinate system due to axial symmetry of the geometry. The actual geometry of the specimen was measured and replicated in the model without cushion. The simulations of but-welding process and the beads were done on simplified geometries. The associated element mesh is shown in Fig. 3. The finite element mesh contains 2048 elements and 2132 nodes. Solid elements were employed to simulate the thermo-elastic-plastic behavior.

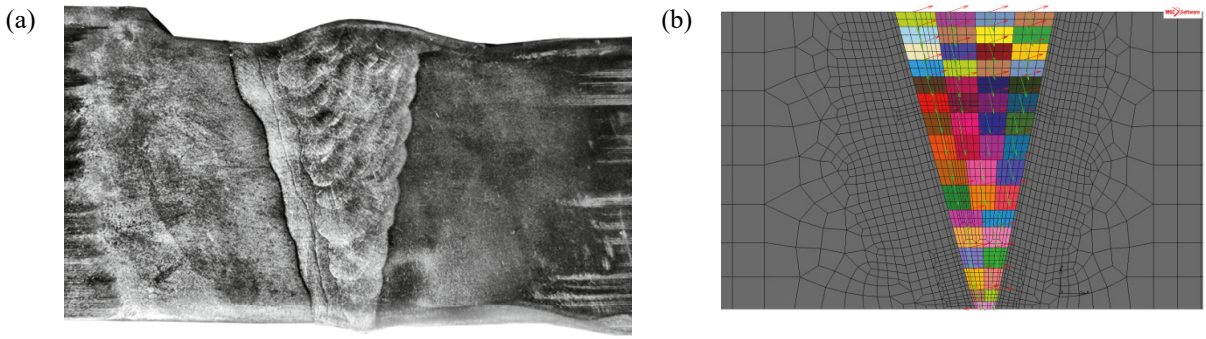


Fig. 3. (a) Investigated specimen; (b) FE mesh of welding simulation.

In order to capture the correct microstructure evolution, a number of material properties are required for present simulations. The elastic behavior is modelled using the isotropic Hooke's rule with temperature-dependent Young's modulus. The thermal strain is considered using thermal expansion coefficient. The yield criterion is the Von Mises yield surface. In the model, the strain hardening is taken into account using the isotropic Hooke's law. During the welding process, besides the elastic, plastic and thermal strains, the strains due to solid-state phase transformation and creep potentially give some contributions to the total strain. Because stainless steel has no solid-state phase transformation during cooling and the heating time is relatively short, it can be expected that the strains due to phase transformation and creep can be neglected in the present simulation.

In the case of girth welding, the direction of the temperature gradient changes inside each pass and also from one pass to the next. Grains tend to follow the direction of the local temperature induced deformation gradient. Fig. 4. represents the deformation gradient distributions of the model after welding.

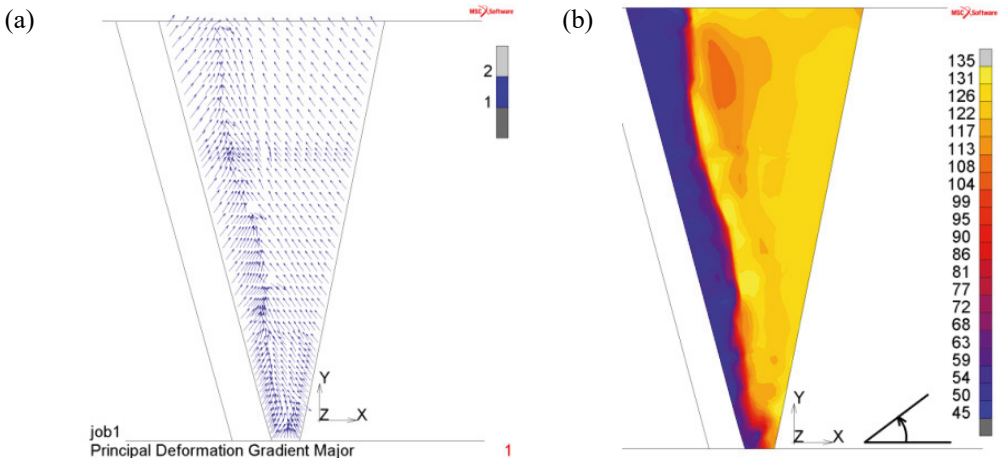


Fig. 4. (a) Modelled orientations as vectors; (b) Contour plots of modelled orientation (45-135°).

## 3. Simulation of ultrasonic inspection

Simulations were used to determine parameters of ultrasonic examination, especially parameters of probes and scan plan and also in results analysis. It is important to verify applicability of probes and method on the test block, which was known defects. Simulations are very useful for verifying of propagation of ultrasonic signal in weld area, especially with limited movement of probe.

In this paper, CIVA 2015a software was used to model the phased array ultrasonic inspection. The CIVA software allows bulk wave beam field predictions using the elastic-dynamics pencil method and defect response predictions using SOV, Kirchhoff and GTD models for beam and defect interaction. The software has the ability to compute delay laws for PAUT setups and the facility to overlay resulting beam profiles and beam/defect responses onto the model of the part. Components requiring defect response predictions need to be drawn in two-dimensional profile in the CIVA software. The two-dimensional axial symmetry profile of the specimen was replicated in CIVA, after this profile was extruded to create the three-dimensional solid model. For the axial symmetry model, all sides are color-coded as front, back, side, and interface so that the ultrasonic probe attached itself properly, and the beam field and defect response predictions were calculated correctly (Fig. 5.).

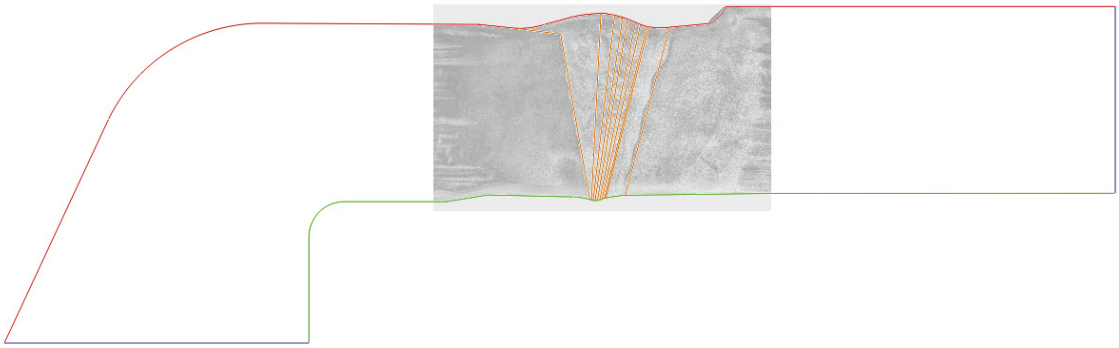

Fig. 5. 2D axial symmetry profile of the steam generator collector.

Regarding the software analysis, the weld has been defined as it is shown in Fig. 6.b, based on the aforementioned grain orientation FEA simulation. The eleven zones shown in the two-dimensional profile consist of two base steel zones and nine weld zones with different grain orientation. Each is assigned the appropriate ultrasonic velocity as measured for the base and weld steels. The anisotropy of the weld materials results of the dependence of the ultrasonic velocity to the direction of propagation and is expressed with the elastic constants by Liu et al. (2007). One set of parameters for equivalent welding material (AISI 316L) has been found in the literature by Tabatabaeipour et al. (2010). Elastic constants used in this study are given in Table 1.

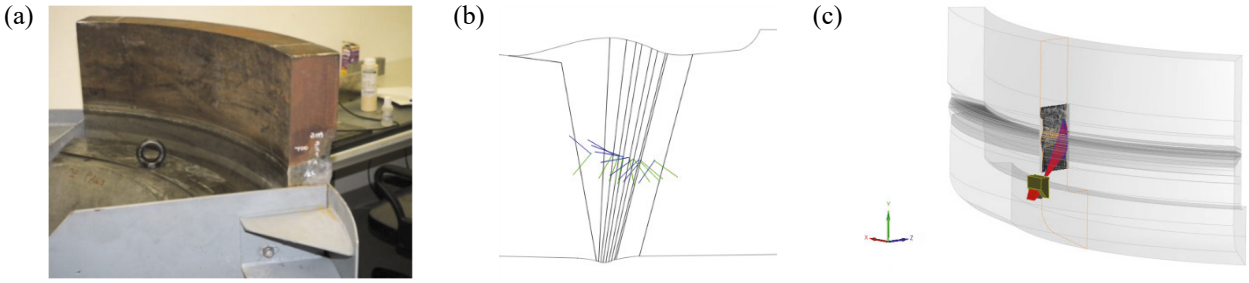


Fig. 6. (a) DMW specimen; (b) Zones of Civa model; (c) 3D solid model.

The base metals (08H18N10T and 22K) around is assumed to be homogeneous and isotropic. The velocity of longitudinal waves is 5660 and 5900 m/s while shear waves propagate at 3120 and 3230 m/s. Caused by the absorption linked to the viscosity of the medium and the scattering of the wave due to the constitutive macroscopic grains, the attenuation represents an energy loss due to the structure of the weld and implies a decrease of the ultrasonic signal. The attenuation was evaluated experimentally, with a reference specimen and in this study was used 0.09 dB/mm attenuation coefficient for isotropic austenitic and weld metals at 2.25 MHz. The model parameters selected match closely with actual experimental parameters. The simulation was performed using linear 32 elements 2.25L32-A5 (24x24 mm) phased array probe emitting a shear wave with flat contact surface wedge. The wedge made of Rexolite plastic with incidence angle of 39°.

Table 1. Elastic constants of welding material

| | $C_{11}$ | $C_{22}$ | $C_{33}$ | $C_{12}$ | $C_{23}$ | $C_{31}$ | $C_{44}$ | $C_{55}$ | $C_{66}$ |
|---|---|---|---|---|---|---|---|---|---|
| SMAW metal | 258.5 | 225.1 | 208.9 | 178.7 | 112.9 | 131.8 | 115.3 | 101.1 | 74.2 |
| GTAW metal | 278.6 | 254.9 | 247.2 | 173.7 | 112.1 | 148.1 | 106.5 | 73.9 | 74.3 |

The defect distribution details in the steam generator nozzle DMW specimen (Fig. 6.a) are provided in Table 2. Defects in the specimen are located in the weld and some specific defects are positioned on different interfaces (22K material to the 1st buttering layer, 1st buttering layer to 2nd buttering layer). As can be seen there are 10 artificial defects of the height from 4.9 to 9.9 mm. The Fig. 7. shows the types of defect, namely (a) A-type and (b) B-type.

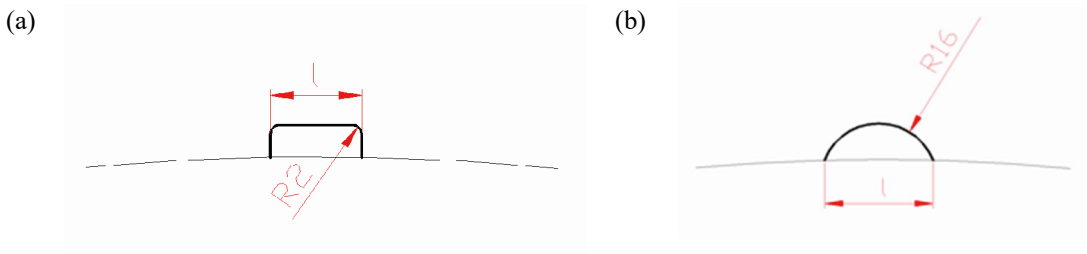


Fig. 7. type of defect: (a) A-type; (b) B-type.

Table 2. Defect locations and dimensions

| Defect number: | 1 | 2 | 3 | 4 | 5 | 6 | 7 | 8 | 9 | 10 |
|---|---|---|---|---|---|---|---|---|---|---|
| Type | A | A | B | B | B | B | B | A | A | A |
| Dimension [mm] | 14.9x4.9 | 20x6.9 | 31x9.9 | 26x6.6 | 33x7.2 | 30x7.6 | 30x8.6 | 19.9x7 | 60x9 | 14.9x5 |
| Location [mm] | WCL+11.8 | WCL+12.3 | WCL | WCL | WCL | WCL | WCL+2 | WCL+11.1 | WCL | WCL+11.6 |
| Till [°] | 18 | 18 | 0 | 0 | 10 | 10 | 0 | 18 | 0 | 18 |
| Skew [°] | 0 | -2.8 | 0 | 0 | -1.4 | -1 | 1.4 | 0 | 0 | 0 |

In this simulation, the transducer was located in a specific position from weld centerline (65 mm) at the austenitic material side to detect the defect and a sectorial scan with range 40° to 65° was performed. The “half-skip” sound path interaction with the defect was chosen in the computation parameters. The side drilled hole (SDH), located in the stainless steel reference specimen, was modeled as a cylindrical flaw and has been chosen as the reference defect. Its SDH echo amplitude was the reference for the 1-10 defect corner echoes.

## 4. Comparison between experimental and modelling

The Fig. 7. represents the measured echoes on B-scan image obtained for an elastic transverse wave propagating from the 08H18N10T stainless.

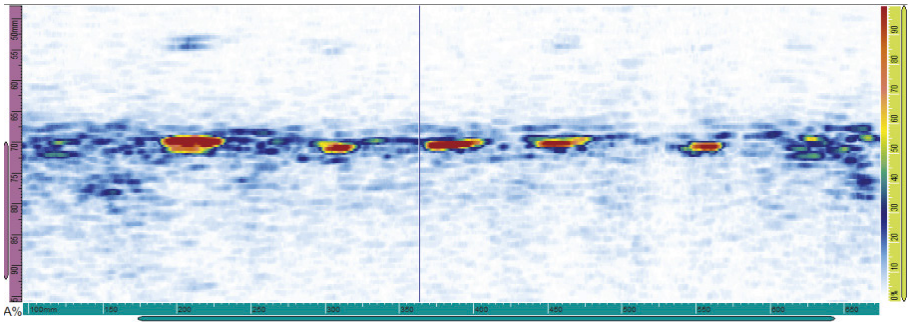

Fig. 8. Measured B-scan image (gain 10dB).

Practical examples of defect indications on S-scans measured for index offset 65 mm can be seen in Fig. 9.a and Fig. 10.a. Appropriate CIVA version 2015a simulation results for the A and B type defect number 2 and 4 can be seen in Fig. 9.b and Fig. 10.b. The amplitudes of the simulated and measured echoes of defects are given in Table 3.

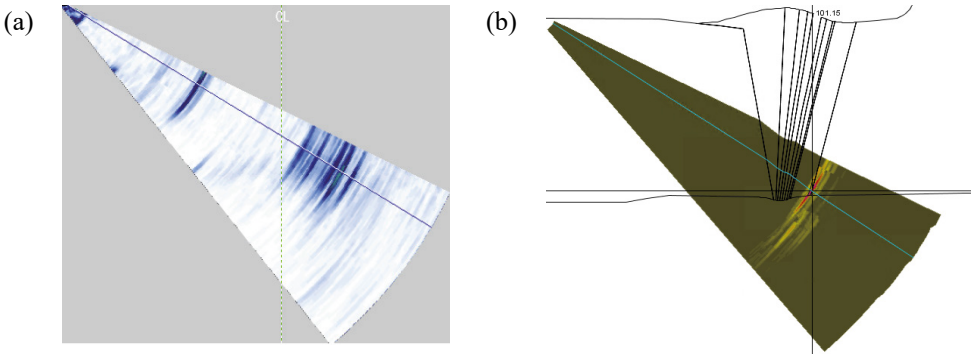


Fig. 9. PAUT examination (a) and CIVA simulation; (b) sectorial scanning results for defect 2.

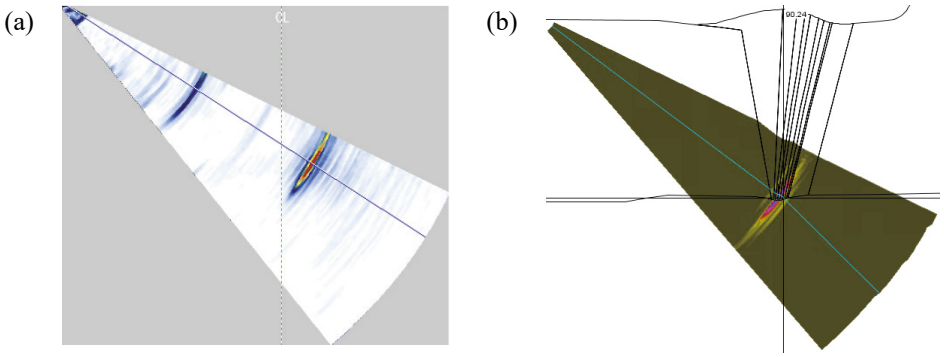


Fig. 10. PAUT examination (a) and CIVA simulation; (b) sectorial scanning results for defect 4.

Table 3. Simulated and experimental amplitudes in dB

| Defect number | 1 | 2 | 3 | 4 | 5 | 6 | 7 | 8 | 9 | 10 |
|---|---|---|---|---|---|---|---|---|---|---|
| Experiment | NA | -15.7 ± 0.6 | -5.1 ± 0.5 | -5.9 ± 0.3 | -2.6 ± 0.4 | -7.6 ± 0.5 | -6.2 ± 0.3 | -16.6 ± 0.2 | -14.4 ±0.4 | -17.2 ± 0.2 |
| CIVA | -9.6 | -10.7 | -4.8 | -5.1 | -2.7 | -7.2 | -6.1 | -12.5 | -13.5 | -11.6 |

The simulations results in Table 3. present a very good agreement with the experiments in case of type B defects, but the maximal difference is 5,6 dB in case of type A defect when the wave travels through the whole welded zone, so further investigations are necessary to implement real attenuation model.

## 5. Conclusion

The goal of the MAPAID project is to model and validate PAUT techniques for inspection of DMWs of nuclear power plants in order to predict ultrasonic propagation in DMW and then to optimize the PAUT inspection of this complex materials. This paper gives an overview of the first results of the developed method. During our research we carried out the simulation of the phase array ultrasonic inspection of the artificial flows in a muck-up of VVER-440 steam generator lower end nozzle. The simulations have been established to examine the defect index most appropriate index offset and angles of irradiation longitudinal and transversal inspection for an artificial defect with specific orientation. The results of the simulation of the S-scan inspections show good agreement with the test results. However a simulation cannot take into account every little difference, only that has been prepared for. It can be concluded that the available and presented simulation method can support the test configuration plan and can improve the evaluation of the results.

## 6. Acknowledgements

The presented work was carried out as a part of the NUGENIA+ "Preparing NUGENIA for HORIZON2020" project that has been founded by the European Community's Seventh Framework Program under grant agreement no 604965.

## References

Skoumalová, Z., Keilová, E., 2014. Investigation of Dissimilar Metal Weld Behavior, Materials Science Forum 782, 149-154.

Kolkoori, S., 2014. Quantitative Evaluation of Ultrasonic Wave Propagation in Inhomogeneous Anisotropic Austenitic Welds using 3D Ray Tracing Method: Numerical and Experimental Validation, PhD Dissertation, BAM.

Moysan, J., Apfel, A., Corneloup, G., Chassignole, B., 2003. Modelling the grain orientation of austenitic stainless steel multipass welds to improve ultrasonic assessment of structural integrity, International Journal of Pressure Vessels and Piping 80, 77-85.

Liu, Q., Wirdelius, H. 2007. A 2D model of ultrasonic wave propagation in an anisotropic weld, NDT&E International 40, 229–238.

Tabatabaeipour, S.M., Honarvar, F., 2010. A comparative evaluation of ultrasonic testing of AISI 316L welds made by shielded metal arc welding and gas tungsten arc welding processes, Journal of Materials Processing Technology 210(8), 1043-1050.